International Forum on Aeroelasticity and Structural Dynamics
IFASD 2019
9-13 June 2019, Savannah, Georgia, USA

MANEUVER LOAD ALLEVIATION OF FLEXIBLE AIRCRAFT THROUGH CONTROL ALLOCATION: A CASE STUDY USING X-HALE

Molong Duan[*1], **John H. Hansen**[1], **Ilya V. Kolmanovsky**[1], **Carlos E. S. Cesnik**[1]

[1]Department of Aerospace Engineering, University of Michigan
Ann Arbor, Michigan USA
Research Fellow, molong@umich.edu
Major, US Air Force, Ph.D. Candidate, hansenjh@umich.edu
Professor, ilya@umich.edu
Professor, cesnik@umich.edu

Keywords: Maneuver load alleviation, control allocation, flexible aircraft

Abstract: The use of high aspect-ratio wings and light structures in aircraft design increases the lift, reduces the drag, and minimizes the weight of the aircraft; however, it inevitably increases aircraft flexibility and requires maneuver load alleviation (MLA) to maintain aircraft structural integrity in aggressive maneuvers. In this paper, a control allocation scheme is proposed that redistributes the control actions from an existing aircraft controller, in a way that the load (and other flexible states) at critical stations are constrained while the rigid body trajectory remains unaffected. The control allocation scheme exploits the preview of maneuver trajectory, the null space established through matrix fraction description of linear model, and a numerical solution of a quadratic programming problem with a basis function decomposition of null space variables. The proposed method is validated by simulations on a linearized model of a flexible X-HALE aircraft. The proposed MLA through control allocation approach is shown to avoid the violation of load bounds without changing the rigid body response of the aircraft.

1 INTRODUCTION

The design for aircraft intended to fly at high altitude with a long endurance (HALE) typically involves long, slender wings with a high aspect ratio and light structure. Both features increase the energy efficiency, thus maximizing the endurance or range of the aircraft. The higher aspect ratio increases lift and reduces induced drag; the lighter structure results in less mass which means that less lift is needed to keep the aircraft airborne. Though high aspect-ratio wings and light structures enhance the energy efficiency, they inevitably introduce more structural flexibility. The increased structural flexibility leads to aeroelastic characteristics such as divergence, flutter, and control surface reversal to become more prominent and start occurring at lower airspeeds. Furthermore, the decreased structural strength may lead to structural yielding or failure during maneuvering flight. Consequently, methods to alleviate the maneuver loads on aircraft, which is generally referred to as maneuver load alleviation (MLA), become necessary.

Maneuver load alleviation can be achieved through hardware and software approaches. Hardware approaches usually introduce additional mechanical components (wing tip device [1], variable camber flap [2], etc.) to alleviate the loads at critical stations. However, due to the high cost of design, manufacturing, and verification of the hardware solutions, software approaches exploiting the existing control surfaces and thrusters are more widely adopted. The early designs

of software-based MLA system called for symmetrically deflecting the wings (e.g., ailerons, flaps) proportionally to the normal acceleration of the airplane [3]. The use of multiple independent control surfaces has been advocated in [4] to enhance the performance of the MLA system and achieve more precise control of the load. To enable more effective use of multiple control surfaced for MLA, advanced control approaches (e.g., $\mathcal{H}_\infty$ loop shaping [5], recurrent neural networks [6], and model predictive control [7]) have been proposed. One common challenge faced by the software-based MLA method is the balance of load alleviation performance and other fundamental objectives (e.g., trajectory tracking).

For aircraft with more control inputs than the rigid body degrees of freedom (i.e., an input redundant system), control allocation methods provide systematic ways to decouple the primary control objective (e.g., trajectory tracking) and the secondary control objective (e.g., load alleviation). They exploit the input redundancy and decouple the control design process into two stages accounting for the primary and secondary objectives separately [8]. In control allocation literature, the dynamic system's input redundancy is categorized into strong and weak input redundancies. Strong input redundancy occurs in systems in which control inputs can be coordinated in such a way that they do not affect the internal states. Weak input redundancy holds in systems in which this null space condition applies to only outputs [9]. Control allocation methods which exploit strong input redundancy have been previously proposed for the control of rigid aircraft [10]. Frost et al. [11] introduced a flight control framework with optimal control allocation using load constraints and load feedback. Miller and Goodrick [12] proposed a control allocation framework which accounts for tracking performance, trim condition enforcement and critical load limiting. These control allocation methods based on strong input redundancy assume a static relationship between the load and the control inputs and may not be effective in regulating dynamic loads with pronounced transient characteristics as in flexible or very flexible aircraft. For this purpose, control allocation methods that exploit weak input redundancy are needed. Toward this end, Gaulocher et. al. [13] proposed a model predictive control framework to solve for the dynamic optimal control allocation problem considering structural load and actuator saturation. Hashemi and Nguyen [14] proposed an adaptive MLA algorithm which incrementally changes the control input to alleviate the load. However, these methods do not explicitly exploit the structure of input redundancy, thus still introducing the tradeoff between trajectory tracking and load alleviation performance.

In this paper, a dynamic control allocation method for load alleviation is proposed for weakly input redundant flexible aircraft. The contributions of the paper are listed as follows: (i) a load alleviation control structure is proposed to completely decouple the load alleviation function and the nominal flight control of rigid body motion, exploiting the null space of weakly input redundant flexible aircraft, (ii) load alleviation with preview horizon and specified bounds is solved by converting into a quadratic programming problem of a reduced-dimension variable, and (iii) the proposed method is validated in simulation using a linearized model of X-HALE aircraft [15] (shown in Figure 1).

The paper is organized as follows: In Section 2, the mathematical definitions of strong and weak input redundancy are reviewed in reference to a linear flexible aircraft model. The control allocation framework, including the null space generation and load alleviation programming, is presented in Section 3. Simulation results based on a linear model of X-HALE aircraft are reported in Section 4. Concluding remarks are made in Section 5.

Figure 1: X-HALE aircraft developed in University of Michigan [15]

2 BACKGROUND

2.1 Flexible Aircraft Model

Consider a flexible aircraft with n_u-dimensional vector of control inputs u, that includes all the control surfaces and inputs from the thrusters. The outputs of the system are decomposed to n_r-dimensional vector of rigid body outputs y_r (e.g., roll, pitch, yaw and their rates), as well as n_f-dimensional vector of flexible outputs y_f representing the structural deformations of interest. Usually, the flexible outputs are curvatures, bending moments, or load factors at critical stations of the aircraft that are expected to be constrained to specified safe ranges during the maneuver. It is assumed that there are more control input channels than the rigid body outputs ($n_u > n_r$), and that the dynamics of the flexible aircraft around a trim point can be modeled by a linear time-invariant (LTI) model with the state-space representation,

$$\begin{cases} \dot{x} = Ax + Bu, \\ y_r = C_r x, \\ y_f = C_f x, \end{cases} \tag{1}$$

where the internal state $x \in R^{n_x}$ represents the rigid and flexible states of the aircraft, as well as other states necessary to account for aerodyamic and aeroelastic effects. Note that the system is assumed to be strictly proper such that there are no feed-through terms. The LTI model can also be represented using transfer function matrices, i.e.,

$$\begin{bmatrix} y_f \\ y_r \end{bmatrix} = \underbrace{\begin{bmatrix} G_{fu}(s) \\ G_{ru}(s) \end{bmatrix}}_{G(s)} u, \tag{2}$$

where $G_{fu}(s)$ and $G_{ru}(s)$ define the partition of $G(s)$, corresponding to the flexible and rigid outputs, respectively.

2.2 Input Redundancy in Flexible Aircraft

Input redundancy is usually exploited in the flight control system of rigid aircraft where the required forces and moments are firstly generated, and then distributed to various control effectors [16]. This control allocation process relies on the control effector matrix B having a nontrivial null space, i.e.,

$$Ker\,(B) \neq 0. \tag{3}$$

Such a property is referred to as strong input redundancy in the control allocation literature. In flexible aircraft, there are usually more states than control inputs such that Eq. (3) is not satisfied, and control allocation algorithms which assume strong input redundancy cannot be used.

Recent developments in control allocation literature [9, 17, 18] generalized the strong input redundancy (input-to-state) defined in Eq. (3) to weak input redundancy (input-to-output), which requires that

$$Ker\,(G_{ru}\,(j\omega)) \neq 0, \text{ for all } \omega. \tag{4}$$

Clearly, strong input redundancy implies weak input redundancy, but not vice versa. The physical meaning of weak input redundancy for flexible aircraft is that there exist different selections of control inputs that yield identical rigid body motions, while the flexible output could be different. Consequently, these control inputs can be manipulated in such a way as to affect the flexible outputs without affecting the rigid body outputs.

In the sequel, an assumption of more control inputs than rigid body outputs ($n_u > n_r$), which is the case for our aircraft models, and which implies weak input redundancy, is made.

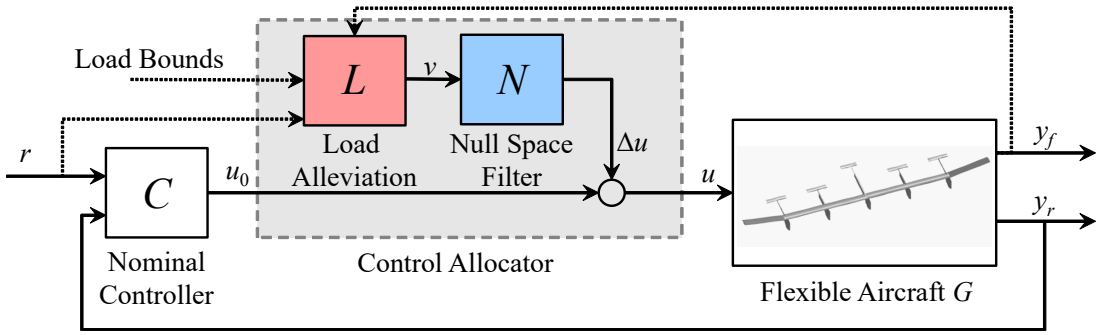

Figure 2: Block diagram of maneuver load alleviation through control allocation

3 MANEUVER LOAD ALLEVIATION THROUGH CONTROL ALLOCATION

The block diagram of the load alleviation through control allocation system is shown in Figure 2. Assume the flexible aircraft G is controlled to track a specified trajectory $r(t) \in R^{n_r}$, $0 \leq t \leq T_p$, for rigid output, where T_p is the preview horizon. The tracking is realized through a nominal controller C. The nominal controller C uses only the rigid body output y_r for feedback, and generates a n_u-dimensional control input u_0. Note that this full dimension nominal controller C directly generates control effect commands and is different from existing nominal flight controller [16, 19] which generate required force and moments. The rigid body motion controlled by C can be realized by infinitely many control input selections due to the nature of weak input redundancy. This redundancy provides the opportunity to change the flexible outputs of the system y_f without affecting tracking performance (i.e., the relationship between r and y_r). Therefore, there are two important functions required in this control allocation framework: (i) null space generation, which guarantees that the control input increment Δu does not change the rigid body output y_r, and (ii) load alleviation calculation, which generates an

auxiliary control signal v to enforce the bounds on y_f using trajectory preview. As Figure 2 illustrates, these two functions are realized through two highlighted blocks N and L. This control allocator incrementally adds to the nominal controller, which simplifies the design and tuning process.

3.1 Computing Null Space Filter, *N*(*s*)

The proposed control allocator adds on to existing nominal controller output, i.e.,

$$u = u_0 + \Delta u \tag{5}$$

so that $G_{ru}(s)u = G_{ru}(s)u_0$, i.e.,

$$G_{ru}(s)\Delta u = 0. \tag{6}$$

Note that $G_{ru}(s)$ used in the subsequent control allocation procedure is a transfer function matrix and not a static matrix as is common in the exiting control allocation literature for strongly input redundant systems. Therefore, to achieve invariant rigid body response, the allocation of Δu needs to be performed throughout the maneuver rather than just for its steady state. Note also that $G_{ru}(s)$ is a fat transfer function matrix as $n_u > n_r$, and $n_e = n_u - n_r$ is defined as the level of input redundancy. Accordingly, $G_{ru}(s)$ can be decomposed into n_r principal control inputs u_p and n_e extra control inputs u_e. Since input channels can always be re-ordered, we assume that the first n_r inputs are the principal control inputs, i.e.,

$$G_{ru}(s) = \begin{bmatrix} G_p(s) & G_e(s) \end{bmatrix}, u = \begin{bmatrix} u_p^{\mathrm{T}} & u_e^{\mathrm{T}} \end{bmatrix}^{\mathrm{T}}, \tag{7}$$

where $G_p(s)$ is an invertible square transfer function matrix and $G_e(s)$ is of dimension $n_r \times n_e$. Using this decomposition, a natural way of satisfying Eq. (6) is to generate control increment Δu as an output of a dynamic system

$$\Delta u = \begin{bmatrix} G_p^{-1}(s)\, G_e(s) \\ -I \end{bmatrix} v, \tag{8}$$

where $v(t)$ is an arbitrary n_e-dimensional signal. However, there is usually no guarantee that $G_p^{-1}(s)G_e(s)$ is stable, thus a more practical and general way is to transform Eq. (8) into a different format, such that all the unstable dynamics are only reflected in the zero dynamics [20]. To accomplish this, $G_p^{-1}(s)G_e(s)$ is expressed using its matrix fractional description [21], i.e.,

$$G_p^{-1}(s)\, G_e(s) = N_G(s)\, D_G^{-1}(s), \tag{9}$$

where $N_G(s)$ and $D_G(s)$ are transfer function matrix polynomials. Using this description, the null space filter, $N(s)$, is defined through a relationship,

$$\Delta u = \underbrace{\begin{bmatrix} -N_G(s) D_0^{-1}(s) \\ D_G(s) D_0^{-1}(s) \end{bmatrix}}_{N(s)} v, \tag{10}$$

where $D_0(s)$ is a square minimal phase denominator transfer function polynomial, which ensures the stability of $N(s)$. From Eqs. (9) and (10), it follows that

$$G_{ru}(s)\Delta u = G_{ru}(s)N(s)v = \underbrace{\left(G_e(s) D_G(s) - G_p(s) N_G(s)\right)}_{=0} D_0^{-1}(s) v = 0, \tag{11}$$

i.e., the output of the null space filter, $N(s)$, will not affect the rigid body outputs independently of the selection of the signal, v. Usually $D_0(s)$ is selected in a form of lowpass filter such that the control effort redistribution only happens at low frequencies where the model is relatively accurate. Note that there exist infinite many $N_G(s)$, $D_G(s)$ and $D_0(s)$ selections. A general guideline is to make sure that the selection yields relatively uniform frequency responses of $N(s)$ (with minimal resonant peaks and anti-resonant frequencies) within the designed bandwidth. To serve this purpose, $D_0(s)$ is selected to be a diagonal transfer function polynomial matrix, i.e.,

$$D_0(s) = \mathrm{diag}\left\{d_1(s),\ d_2(s),\ \ldots,\ d_{n_e}(s)\right\} \tag{12}$$

Note that each $d_i(s)(i = 1, 2, \ldots, n_e)$ serves as the common denominator of the ith column of $N_G(s)$ and $D_G(s)$, thus can be generated by averaging corresponding columns. Defining this average to be φ_i for each column, i.e.,

$$\varphi_i(s) = \frac{1}{n_u}\left(\sum_{k=1}^{n_y} N_G^{(k,i)}(s) + \sum_{k=1}^{n_e} D_G^{(k,i)}(s)\right), \quad (i = 1, 2, \ldots, n_e), \tag{13}$$

where superscript $^{(k,i)}$ indicates the element in kth row and ith column in a transfer function matrix. Accordingly, $d_i(s)$ is selected as

$$d_i(s) = \varphi_{mp,i}(s)\left(\frac{s^2}{\omega_0^2} + 2\frac{\zeta}{\omega_0}s + 1\right), \tag{14}$$

where $\varphi_{mp,i}(s)$ is the minimal phase transformation of $\varphi_i(s)$ by reflecting its right half plane zeros to their mirror locations in the left half plane, and the additional second-order polynomial ensures that $N(s)$ is strictly proper, and sets the control allocation bandwidth to ω_0.

3.2 Maneuver Load Alleviation

With Δu generated as the output of the null space filter, the rigid body output y_r is not affected by the control allocator (i.e., $G_{ru}(s)\Delta u = 0$) and its response is calculated as

$$y_r = G_{ru}C\left(r - y_r\right) \Rightarrow y_r = \left(I + G_{ru}C\right)^{-1} G_{ru}Cr. \tag{15}$$

Similarly, the response of the flexible outputs satisfies,

$$\begin{aligned} &y_f = G_{fu}\left(u_0 + Nv\right) = G_{fu}\left(Cr - Cy_r + Nv\right) \Rightarrow \\ &y_f = \underbrace{G_{fu}C\left[I - \left(I + G_{ru}C\right)^{-1} G_{ru}C\right]}_{H_{fr}(s)} r + \underbrace{G_{fu}N}_{H_{fv}(s)} v, \end{aligned} \tag{16}$$

where $H_{fr}(s)$ and $H_{fv}(s)$ can be realized as LTI systems. To make sure that the $y_f(t)$ lies within bounds y_f^- and y_f^+, the null space signal v must satisfy the condition,

$$y_f^- \leq y_f(t) \leq y_f^+ \Leftrightarrow y_f^- - H_{fr}(s)r \leq H_{fv}(s)v \leq y_f^+ - H_{fr}(s)r. \tag{17}$$

In generating the terms $H_{fr}(s)r$, $H_{fv}(s)v$ in Eq. (17), we assume that $H_{fr}(s)$ and $H_{fv}(s)$ have zero initial conditions since the maneuver starts from trim. Over the specified preview horizon T_p, the discrete-time implementation of LTI systems can be performed through multiplication of Toeplitz matrices, e.g. $y_{fv} \triangleq H_{fv}(s)v$ is expressed as

$$\begin{aligned} &\underbrace{\begin{bmatrix} \mathbf{y}_{fv}^{(1)} \\ \vdots \\ \mathbf{y}_{fv}^{(n_f)} \end{bmatrix}}_{\mathbf{y}_{fv}} = \underbrace{\begin{bmatrix} \mathbf{H}_{fv}^{(1,1)} & \cdots & \mathbf{H}_{fv}^{(1,n_e)} \\ \vdots & \ddots & \vdots \\ \mathbf{H}_{fv}^{(n_f,1)} & \cdots & \mathbf{H}_{fv}^{(n_f,n_e)} \end{bmatrix}}_{\mathbf{H}_{fv}} \underbrace{\begin{bmatrix} \mathbf{v}^{(1)} \\ \vdots \\ \mathbf{v}^{(n_e)} \end{bmatrix}}_{\mathbf{v}}, \\ &\mathbf{H}_{fv}^{(i,k)} = \begin{bmatrix} h_{fv}^{(i,k)}(0) & 0 & 0 & 0 \\ h_{fv}^{(i,k)}(T_s) & h_{fv}^{(i,k)}(0) & 0 & 0 \\ \vdots & \vdots & \ddots & 0 \\ h_{fv}^{(i,k)}(n_T T_s) & h_{fv}^{(i,k)}((n_T-1)T_s) & \cdots & h_{fv}^{(i,k)}(0) \end{bmatrix}, \\ &\mathbf{v}^{(k)} = \begin{bmatrix} v^{(k)}(0) & v^{(k)}(T_s) & \cdots & v^{(k)}(n_T T_s) \end{bmatrix}^{\mathrm{T}},\ k = 1, 2 \ldots, n_e, \\ &\mathbf{y}_{fv}^{(i)} = \begin{bmatrix} y_{fv}^{(i)}(0) & y_{fv}^{(i)}(T_s) & \cdots & y_{fv}^{(i)}(n_T T_s) \end{bmatrix}^{\mathrm{T}},\ i = 1, 2 \ldots, n_f, \end{aligned} \tag{18}$$

where T_s is the sampling time in discrete implementation, $n_T = \lceil T_p/T_s \rceil$ marks the number of samplings required to cover preview horizon T_p, and $\left\{ h_{fv}^{(i,k)}(0),\ h_{fv}^{(i,k)}(T_s), \ldots,\ h_{fv}^{(i,k)}(n_T T_s) \right\}$ is the impulse response of $H_{fv}^{(i,k)}(s)$. Time domain signal $v(t)$ is converted to a vector $\mathbf{v}$, while the LTI system $H_{fv}(s)$ is converted into Toeplitz matrix $\mathbf{H}_{fv}$. Toeplitz matrix $\mathbf{H}_{fr}$ and reference vector $\mathbf{r}$ are created in the same way. Thus, maneuver load alleviation with constraint in Eq. (17) is realized through quadratic programming as

$$\begin{aligned} &\min_{\mathbf{v}} \mathbf{v}^{\mathrm{T}}\mathbf{v}, \\ &\text{s.t. } y_f^- - \mathbf{H}_{fr}\mathbf{r} \leq \mathbf{H}_{fv}\mathbf{v} \leq y_f^+ - \mathbf{H}_{fr}\mathbf{r}. \end{aligned} \tag{19}$$

Note that no a priori guarantees of feasibility of Eq. (19) can be given; the constraints can be relaxed with slack variables to ensure that Eq. (19) is always feasible. Furthermore, basis functions can be exploited to represent v, thereby potentially reducing the computational load.

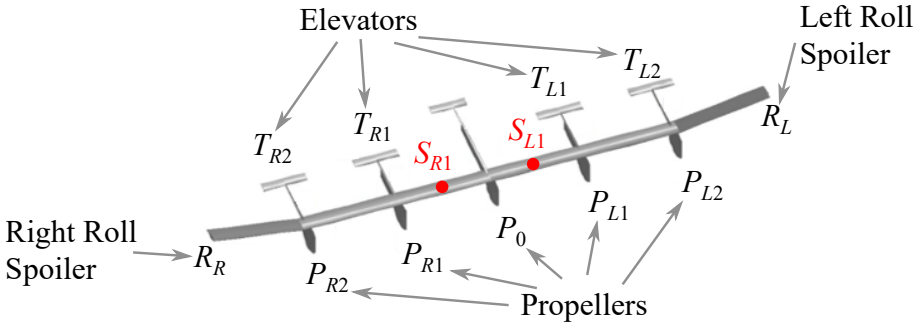

Figure 3: Control inputs and critical stations on X-HALE

4 SIMULATION STUDIES

4.1 X-HALE Modeling and Nominal Control

The proposed method is validated using simulations on X-HALE linearized aircraft model. X-HALE is a very flexible aircraft originally developed for aeroelastic tests [15]. As illustrated in Figure 3, the X-HALE is equipped with four elevators ($T_{L1}, T_{L2}, T_{R1}, T_{R2}$), two roll spoilers ($R_L, R_R$), and five thrusters ($P_0, P_{L1}, P_{L2}, P_{R1}, P_{R2}$). In total, this comprises eleven control inputs to the system, i.e., $n_u = 11$. Accordingly, the control input u is defined as

$$u = \begin{bmatrix} R_L & R_R & T_{L1} & T_{L2} & T_{R1} & T_{R2} & P_0 & P_{L1} & P_{L2} & P_{R1} & P_{R2} \end{bmatrix}^{\mathrm{T}}. \tag{20}$$

The vector of rigid body outputs to be controlled ($n_r = 3$) consists of the roll, pitch, and yaw angular rates, i.e.,

$$y_r = \begin{bmatrix} p & q & r \end{bmatrix}^{\mathrm{T}}. \tag{21}$$

The critical stations to evaluate the flexible outputs are defined as S_{L1} and S_{R1}, see Figure 3. The vector of flexible outputs, y_f, comprises the out-of-plane bending curvatures at the critical stations, i.e.,

$$y_f = \begin{bmatrix} \kappa_{L1} & \kappa_{R1} \end{bmatrix}^{\mathrm{T}}. \tag{22}$$

The linearized model of X-HALE was obtained from the University of Michigan Nonlinear Aeroelastic Simulation Toolbox (UM/NAST), which exploits a strain-based formulation of elastic and rigid-body dynamics [22]. The stiffness of X-HALE was numerically doubled versus the real aircraft so that the resulting model is representative of flexible rather than very flexible aircraft. This limits the shape deformation and is synergistic with the assumption of linear structural dynamics. The linear model is generated at a trimmed condition of straight, level, unaccelerated flight. The trim airspeed is 14 m/s, with an angle of attack of 1.8° at an altitude of 30 m. This is a typical flight condition of X-HALE. At this condition, the wings already have a deformed shape, with an out-of-plane curvature of -0.052 m^{-1} at both inboard wing sections

S_{L1} and S_{R1} (negative curvature indicates an upward bend). The curvature for each of the mid-wing sections is -0.022 m^{-1}. The outboard wing sections have a curvature of -0.007 m^{-1}. Since the steady-state curvature values at the inboard wing sections are larger, those sections were selected as the critical stations of the structure.

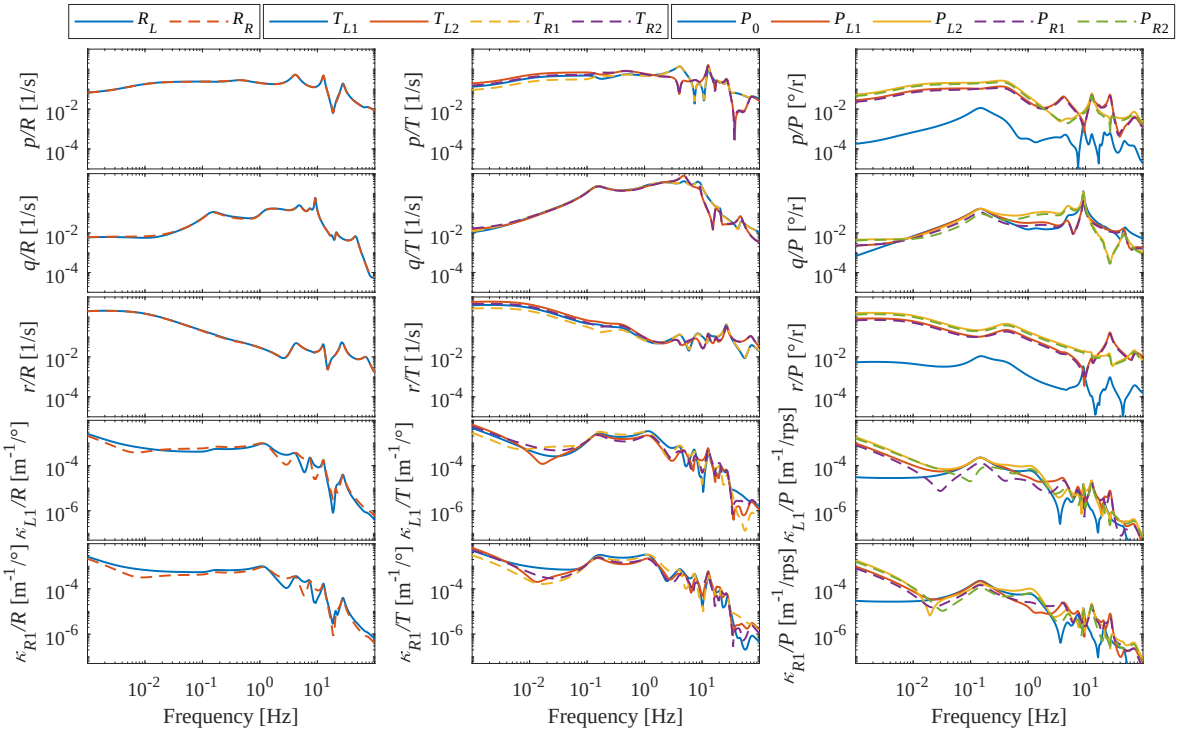

Figure 4: Frequency response of linear X-HALE model

The frequency response of the linear flexible aircraft is shown in Figure 4. Most peaks in Figure 4 correspond to the structural modes of the flexible X-HALE aircraft. Note that the first three rows correspond to the rigid body response (i.e., p, q, r) while the last two rows correspond to the out-of-plane curvature κ_{L1} and κ_{R1} at critical stations S_{L1} and S_{R1}, respectively. The three columns illustrate the control inputs from roll spoilers, elevators, and thrusters, respectively. The left and right roll spoilers affect the rigid body response at almost identical magnitudes, their slight difference arises from the geometric distance difference from the roll spoilers to S_{L1}. The elevators affect the pitch rate q in a very similar way, but the outside elevators T_{L2} and T_{R2} are more capable of introducing roll and yaw compared to the inside elevators due to additional moment. This spatial distribution also affects the response of the thrusters: the outside thrusters P_{L2} and P_{R2} are more capable of affecting roll, yaw and bending curvature, while the central thruster P_0 provides significantly less effect on these outputs. It is also noteworthy that the elevators affect bending curvature more significantly compared to other control inputs. This property may be exploited in the process of control allocation.

The nominal controller C adopts the control structure in [23], and is illustrated in Figure 5. Cascaded proportional/proportional-integral (P/PI) controllers are used to control the roll and pitch, while a proportional controller is used to control the yaw. These P/PI and proportional controllers generate τ_p, τ_q, and τ_r, which inform required control actions for roll, pitch and yaw axes, respectively. Their directions are defined in a way that positive τ_p, τ_q and τ_r induce positive roll, pitch and yaw motion, respectively. The corresponding gains are provided in Table 1. The

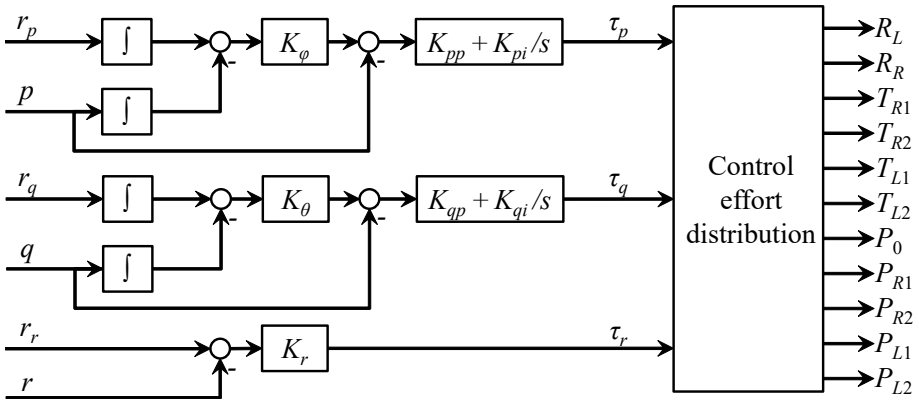

Figure 5: Nominal controller C structure [23]

required control actions are further assigned to each control input as

$$\begin{bmatrix} R_L \\ R_R \end{bmatrix} = \begin{cases} \begin{bmatrix} R_{\max} - R_{\text{trim}} & 0 \end{bmatrix}^{\mathrm{T}} & \text{if } \tau_p \leq -(R_{\max} - R_{\text{trim}}) \\ \begin{bmatrix} -\tau_p & 0 \end{bmatrix}^{\mathrm{T}} & \text{if } -(R_{\max} - R_{\text{trim}}) < \tau_p \leq R_{\text{trim}} \\ \begin{bmatrix} -R_{\text{trim}} & \tau_p - R_{\text{trim}} \end{bmatrix}^{\mathrm{T}} & \text{if } R_{\text{trim}} < \tau_p \leq R_{\max} + R_{\text{trim}} \\ \begin{bmatrix} -R_{\text{trim}} & R_{\max} \end{bmatrix}^{\mathrm{T}} & \text{if } R_{\max} + R_{\text{trim}} < \tau_p \end{cases}$$
$$\begin{aligned} T_{L1} &= T_{R1} = \tau_q, \\ T_{L2} &= \tau_q + K_{p,\text{tail}}\tau_p, \\ T_{R2} &= \tau_q - K_{p,\text{tail}}\tau_p, \\ P_0 &= 0, \\ P_{L1} &= P_{L2} = \tau_r, \\ P_{R1} &= P_{R2} = -\tau_r. \end{aligned} \tag{23}$$

Note that the original control effort distribution in [23] actuated the four elevators symmetrically for the pitch motion, while adopting differential thrust between the left-side and right-side thrusters for the yaw motion. In comparison to this original approach, two modifications are made. Firstly, the spoiler inputs are asymmetrically defined for the roll motion with four different configurations considering τ_p and the trimmed condition, R_{trim}. Note that the trimmed condition of the roll spoilers is assumed to be a positive deflection of R_L and zero deflection of R_R. This modification arises from the roll spoilers' physical motion range from 0° to 30° ($R_{\max}$). Secondly, the roll control action τ_r (scaled by $K_{p,\text{tail}}$) is routed asymmetrically to the outboard elevators T_{L2} and T_{R2}, to enhance the roll control authority of the aircraft. This nominal controller design already includes a heuristic baseline control allocation structure, which is based on standard manipulation methods of the throttle, roll, pitch, and yaw in stability augmentation systems. Also, this design only uses the feedback of the rigid body angular rates, which satisfies the specification of separating the rigid and flexible outputs y_r and y_f in Figure 2.

Table 1: Gains of nominal controller C

K_ϕ [s^{-1}]	K_{pp} [s]	K_{pi}	K_θ [s^{-1}]	K_{qp} [s]	K_{qi}	K_r[s]	$K_{p,\text{tail}}$
2.5	1.3	3	23	0.01	0.1	200	0.4

4.2 Simulation Examples of MLA through Control Allocation on X-HALE

The maneuver load alleviation scheme developed in Section 3 is verified using the linear X-HALE model and nominal control law from Section 4.1. As shown in Figure 2, the null space

filter is generated based on X-HALE linearized model, and the quadratic programming problem in Eq. (19) is formed, with curvature bounds on critical stations S_{L1} and S_{R1} set to $\pm 0.056\,\mathrm{m}^{-1}$. The quadratic programming problem is solved using the active-set method; the computed null space variable, v, is used to establish Δu, which incrementally modifies the control surfaces on top of the nominal controller. Two different maneuvers are considered in the simulations:

(i) Climb maneuver: The reference trajectory involves a pitch up two seconds after the simulation starts with a pulse of $8.2°/\mathrm{s}$, intended to achieve $10°$ of pitch in one second and holding for nine seconds before leveling off in one additional second. This results in a climb of 15 meters.

(ii) Climbing turn maneuver: The reference trajectory directs to bank the aircraft and change the yaw rate one second after the simulation starts. A pulse of $30°/\mathrm{s}$ is given for the roll rate and a yaw rate of $15°/\mathrm{s}$ is established in one second. The bank angle and yaw rate are held for five seconds before the reference reverses the initial trajectory over one second to return to zero bank angle on a new heading. This results in a target heading angle change of $90°$. The longitudinal reference command of the trajectory is the same as in the climb maneuver.

Additional trajectories which did not include a pitch component were explored but did not sufficiently excite the bending curvature beyond the bound. Therefore, the climbing turn maneuver was chosen to demonstrate the functionality of the MLA system for multi-axial maneuvers.

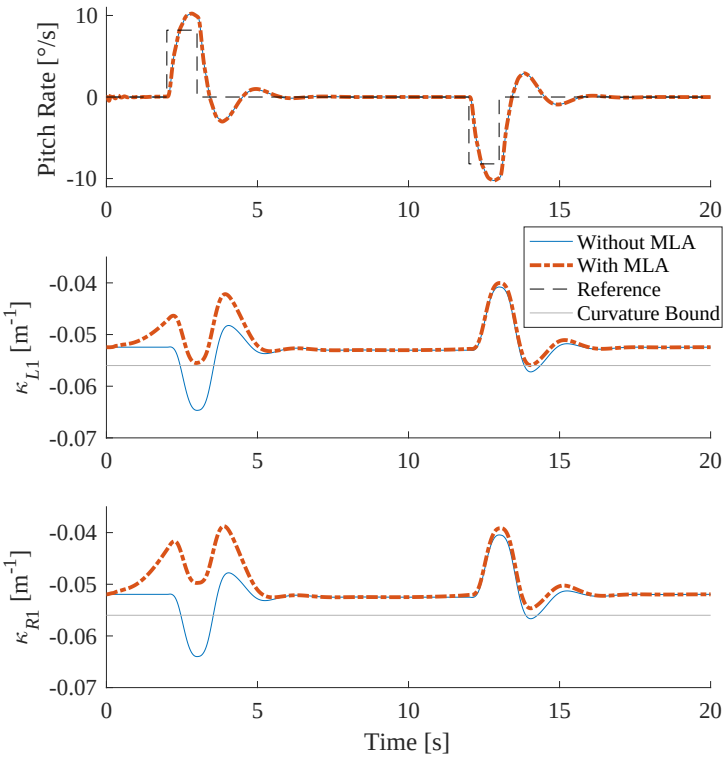

Figure 6: Responses of pitch rate and wing root bending curvature for climb maneuver with and without MLA

The pitch angle response and the bending curvature at the critical stations are shown in Figure 6. Roll and yaw responses are not shown in Figure 6 since pitch control is designed in a decoupled way as discussed in Section 4.1. Note that the pitch response with and without the

MLA are identical, indicating that the trajectory tracking performance is not affected by MLA. This benefit arises from utilizing the null space which exploits the weak input redundancy of the system. This is more powerful and general compared to traditional control allocation based on strong input redundancy. Note that the bending curvatures κ_{L1} and κ_{R1} violate the specified constraints without MLA through control allocation and are kept within the bounds by using our MLA scheme. The curvatures with MLA converge to the curvatures without MLA in regions where constraints are not violated. This is consistent with the objective function in Eq. (19), where changes to the nominal control signal are being minimized.

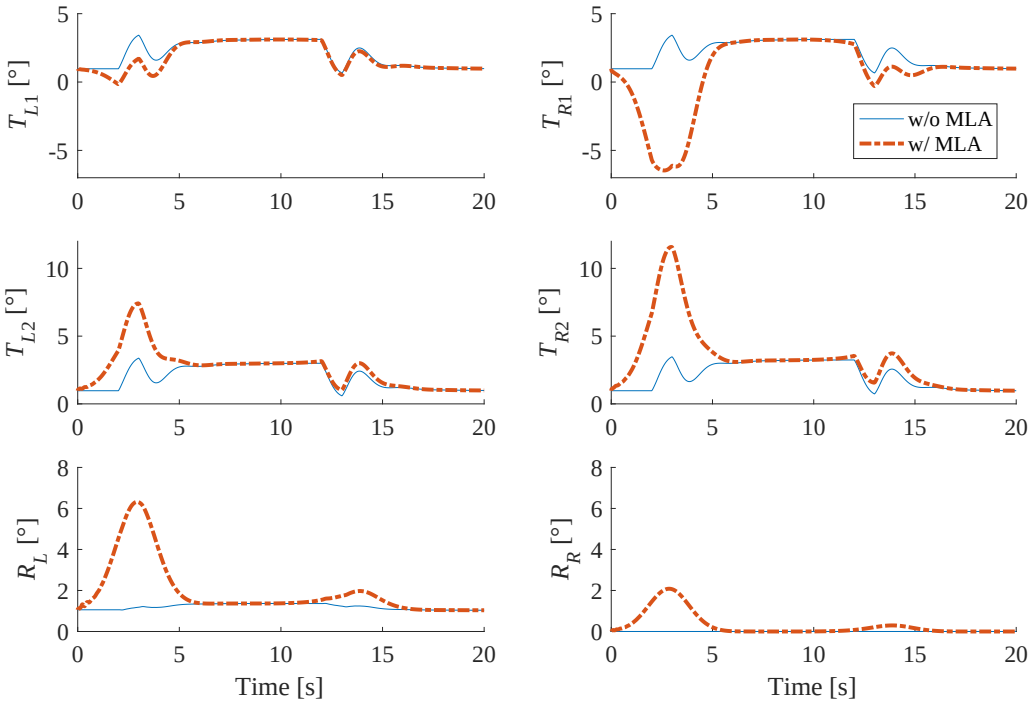

Figure 7: Time histories of elevator and roll spoiler inputs for climb maneuver with and without MLA

The time histories of the elevator and roll spoiler inputs are shown in Figure 7. The incremental changes to the thruster inputs were less than one percent of the normalized throttle signal and, therefore, are not shown. The control inputs of the inner elevators (T_{L1} and T_{R1}) are decreased to reduce the bending curvature at the wing root while the deflection of the outside elevators (T_{L2} and T_{R2}) is increased. The roll spoilers are also engaged symmetrically to move the lift away from the wing tips. This redistribution of lift may at first seem counter-intuitive compared to traditional MLA systems where most of the control efforts are redistributed to the inward control surfaces. However, this behavior aligns with the fact that the X-HALE model has straight wings, with no taper. Also, the X-HALE mass is distributed across the wingspan, in contrast to the heavy fuselage in commercial aircraft. Therefore, the changes result in a more distributed lift profile throughout the middle two-thirds of the wing, rather than the center. Note the proposed method assumes a preview of T_p window, which results in incremental changes to the control input that start to reduce the bending curvature before the maneuver is commanded, in anticipation of the large change in curvature caused by the pitch-up motion.

The tracking performance and the flexible outputs at the critical stations for the climbing turn maneuver are shown in Figure 8. The pitch response is similar to the first maneuver, which

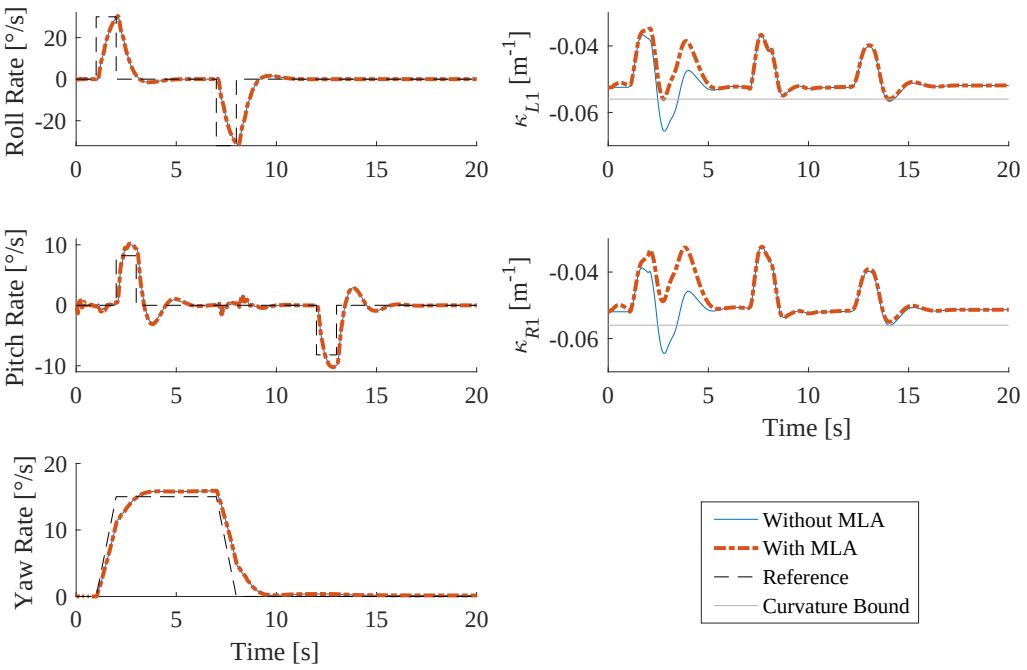

Figure 8: Responses of rigid body motion and wing root bending curvatures for climbing turn maneuver with and without MLA

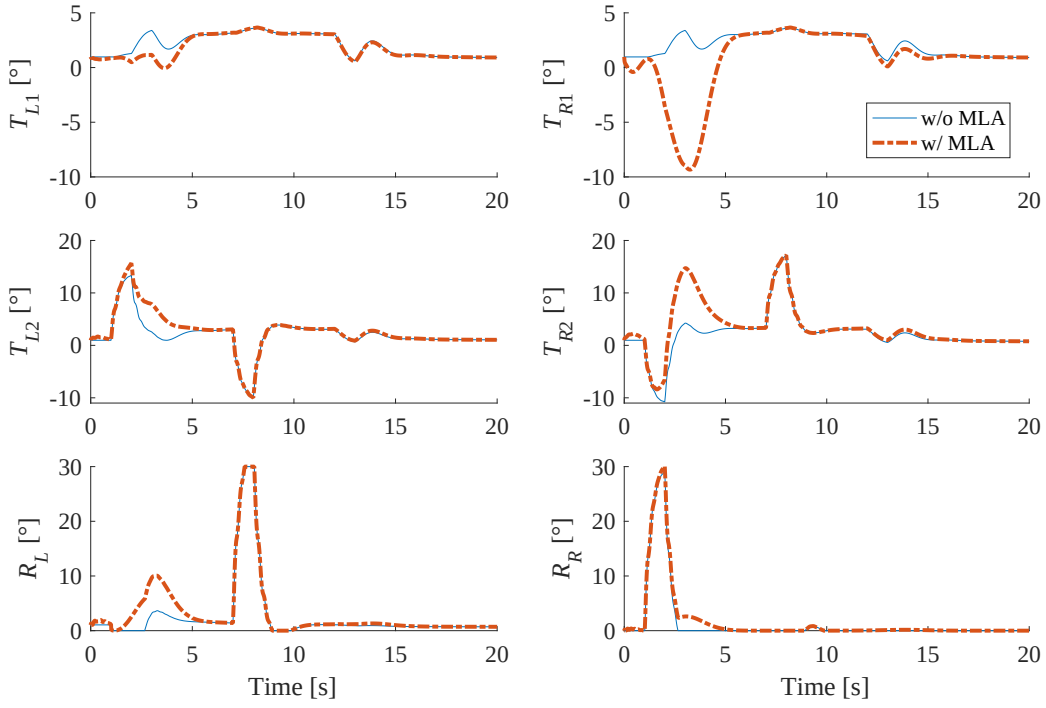

Figure 9: Time histories of elevator and the roll spoiler inputs for climbing turn maneuver with and without MLA

confirms the decoupled design of the nominal controller was not compromised by the control allocation. As in the climb, all rigid body responses with and without MLA are identical, verifying the effectiveness of the null space filter in the control allocation. The bending curvature excursions are restricted within bounds by the proposed approach. The time histories of the tail and roll spoiler inputs are shown in Figure 9. At the beginning of the maneuver, the left roll spoiler, which is not heavily used by the nominal controller at this instant, is engaged to alleviate the load. During this maneuver, the inner elevators (T_{L1} and T_{R1}) have more negative deflection to reduce the bending curvature at the wing root while the deflections of the outside elevators (T_{L2} and T_{R2}) are increased. This also arises from the redistribution of lift forces to the outside control surfaces, due to the same reasons as for the first maneuver.

5 CONCLUSIONS

A novel maneuver load alleviation scheme for flexible aircraft is proposed which exploits control allocation. The aircraft is assumed to have more control input channels compared to the rigid body outputs, which satisfies the weak input redundancy condition. Exploiting the structure of input redundancy, our control allocation approach involves incrementally modifying the control inputs (i.e., elevator inputs, thrusters, and roll spoilers) generated by a nominal controller without changing the rigid body response while providing maneuver load alleviation. This decoupling of rigid body response is achieved by establishing a dynamic null space with a reduced-dimension null space variable. The manipulation of this null space variable affects only the flexible output, and is thus optimized to reduce the load on critical stations. The optimization assumes a preview horizon longer than a typical maneuver, and is organized into a quadratic programming problem with a basis function decomposition of null space variables. The quadratic programming problem minimizes the control re-allocation due to MLA while enforcing load constraints. The proposed method is validated in simulations of climbing and climbing turn maneuvers using a linear model of flexible aircraft X-HALE developed in University of Michigan. The load alleviation scheme is shown to avoid the violation of load bounds without changing the rigid body dynamics of the aircraft. The extension of the method to linear parameter varying and nonlinear systems will be explored in a future work.

6 REFERENCES

[1] Fonte, F., Toffol, F., and Ricci, S. (2018). Design of a Wing Tip Device for Active Maneuver and Gust Load Alleviation. In *2018 AIAA/ASCE/AHS/ASC Structures, Structural Dynamics, and Materials Conference*. p. 1442.

[2] Urnes, J. and Nguyen, N. (2013). A Mission Adaptive Variable Camber Flap Control System to Optimize High Lift and Cruise Lift to Drag Ratios of Future N+3 Transport Aircraft. In *51st AIAA Aerospace Sciences Meeting including the New Horizons Forum and Aerospace Exposition*. p. 214.

[3] White, R. J. (1971). Improving the Airplane Efficiency by Use of Wing Maneuver Load Alleviation. *Journal of Aircraft*, 8(10), 769–775.

[4] Yang, Y., Wu, Z., and Yang, C. (2013). Control Surface Efficiency Analysis and Utilization of an Elastic Airplane for Maneuver Loads Alleviation. In *54th AIAA/ASME/ASCE/AHS/ASC Structures, Structural Dynamics, and Materials Conference*. pp. 1–7.

[5] Yagil, L., Raveh, D. E., and Idan, M. (2018). Deformation Control of Highly Flexible Aircraft in Trimmed Flight and Gust Encounter. *Journal of Aircraft*, 55(2), 829–840.

[6] Li, H., Zhao, Y., and Hu, H. (2016). Adaptive Maneuver Load Alleviation via Recurrent Neural Networks. *Journal of Guidance, Control, and Dynamics*, 40(7), 1824–1831.

[7] Pereira, M. d. V., Kolmanovsky, I., Cesnik, C. E., et al. (2019). Model Predictive Control Architectures for Maneuver Load Alleviation in Very Flexible Aircraft. In *AIAA Scitech 2019 Forum*. p. 1591.

[8] Johansen, T. A. and Fossen, T. I. (2013). Control Allocationa Survey. *Automatica*, 49(5), 1087–1103.

[9] Zaccarian, L. (2009). Dynamic Allocation for Input Redundant Control Systems. *Automatica*, 45(6), 1431–1438.

[10] Durham, W., Bordignon, K. A., and Beck, R. (2016). *Aircraft Control Allocation*. Chichester, UK: John Wiley & Sons, Ltd.

[11] Frost, S. A., Bodson, M., Burken, J. J., et al. (2015). Flight Control with Optimal Control Allocation Incorporating Structural Load Feedback. *Journal of Aerospace Information Systems*, 12(12), 825–835.

[12] Miller, C. J. and Goodrick, D. (2017). Optimal Control Allocation with Load Sensor Feedback for Active Load Suppression, Experiment Development. In *AIAA Guidance, Navigation, and Control Conference*. p. 1719.

[13] Gaulocher, S. L., Roos, C., and Cumer, C. (2007). Aircraft Load Alleviation During Maneuvers Using Optimal Control Surface Combinations. *Journal of Guidance, Control, and Dynamics*, 30(2), 591–600.

[14] Hashemi, K. E. and Nguyen, N. T. (2018). Adaptive Maneuver Load Alleviation for Flexible Wing Aircraft with Nonminimum Phase Zeros. In *2018 AIAA Guidance, Navigation, and Control Conference*. p. 619.

[15] Cesnik, C. E. S., Senatore, P. J., Su, W., et al. (2012). X-HALE: A Very Flexible Unmanned Aerial Vehicle for Nonlinear Aeroelastic Tests. *AIAA journal*, 50(12), 2820–2833.

[16] Oppenheimer, M. W., Doman, D. B., and Bolender, M. A. (2010). Control Allocation. In W. S. Levine (Ed.), *The Control Handbook*, chap. 8. Boca Raton: CRC Press, 2 ed., pp. 8–24.

[17] Duan, M. and Okwudire, C. (2018). Proxy-Based Optimal Control Allocation for Dual-Input Over-Actuated Systems. *IEEE/ASME Transactions on Mechatronics*, 23(2), 895–905.

[18] Duan, M. and Okwudire, C. E. (2019). Connections between Control Allocation and Linear Quadratic Control for Weakly Redundant Systems. *Automatica*, 101, 96–102.

[19] Yildiz, Y. and Kolmanovsky, I. (2011). Stability Properties and Cross-Coupling Performance of the Control Allocation Scheme CAPIO. *Journal of Guidance, Control, and Dynamics*, 34(4), 1190–1196.

[20] Duan, M. and Okwudire, C. (2017). Proxy-Based Optimal Dynamic Control Allocation for Multi-Input, Multi-Output Over-Actuated Systems. In *Proceedings of the ASME 2017 Dynamic Systems and Control Conference*. Tyson, VA: ASME, p. V001T03A005.

[21] Kailath, T. (1980). *Linear Systems*, vol. 156. Prentice-Hall Englewood Cliffs, NJ.

[22] Su, W. and Cesnik, C. E. S. (2011). Strain-Based Geometrically Nonlinear Beam Formulation for Modeling Very Flexible Aircraft. *International Journal of Solids and Structures*, 48(16-17), 2349–2360.

[23] Pang, Z. Y. (2018). *Modeling, Simulation and Control of Very Flexible Unmanned Aerial Vehicle*. Ph.D. thesis, University of Michigan, Ann Arbor.

COPYRIGHT STATEMENT